ChemPubSoc Europe

DOI: 10.1002/cphc.201300944

The Geometric Structure of Silver-Doped Silicon Clusters

Yejun Li,[a] Jonathan T. Lyon,[c, d] Alex P. Woodham,[b, d] André Fielicke,*[b, d] and Ewald Janssens*[a]

Cationic silver-doped silicon clusters, Si_nAg^+ ($n=6$–15), are studied using infrared multiple photon dissociation in combination with density functional theory computations. Candidate structures are identified using a basin-hopping global optimizations method. Based on the comparison of experimental and calculated IR spectra for the identified low-energy isomers, structures are assigned. It is found that all investigated clusters have exohedral structures, that is, the Ag atom is located at the surface. This is a surprising result because many transition-metal dopant atoms have been shown to induce the formation of endohedral silicon clusters. The silicon framework of Si_nAg^+ ($n=7$–9) has a pentagonal bipyramidal building block, whereas the larger Si_nAg^+ ($n=10$–12, 14, 15) clusters have trigonal prism-based structures. On comparing the structures of Si_nAg^+ with those of Si_nCu^+ (for $n=6$–11) it is found that both Cu and Ag adsorb on a surface site of bare Si_n^+ clusters. However, the Ag dopant atom takes a lower coordinated site and is more weakly bound to the Si_n^+ framework than the Cu dopant atom.

1. Introduction

Silicon is the most important element in the microelectronics industry. With the ongoing downscaling of components towards nanoelectronics devices, there is a significant interest in the properties of nanometer-sized silicon particles.[1,2] Silicon clusters have been extensively investigated experimentally[3–7] and theoretically.[8–15] Contrary to the isolobal carbon, silicon favors sp^3 hybridization rather than sp^2 hybridization, which leads to rather asymmetric and reactive structures for pure silicon clusters and makes the formation of cagelike structures unstable.[16] One possible solution to overcome this deficiency is to add transition-metal dopant atoms to the silicon clusters, which is known to induce the formation of stable and unreactive cagelike structures.[17–22] It is, however, not clear if coinage-metal (Cu, Ag, and Au) dopants can induce cage formation for these silicides.

Knowledge of the precise structure of a cluster is vital for the understanding of its chemical and physical behavior. The introduction of a single dopant atom in silicon clusters may have a significant influence on the geometric structures of the clusters, and hence also on the electronic, optical, and chemical properties. An approach that has proved to be successful for the structural assignment of isolated gas-phase clusters is combining infrared multiple photon dissociation (IR-MPD) spectroscopy of cluster–rare gas complexes with density functional theory (DFT) calculations.[18,23–27]

The interest in coinage-metal silicides is primarily motivated by the associated consequences of silicide formation at the metal/silicon interface of semiconductor and microelectronics devices. Numerous solid-state experimental techniques have been implemented to detect metal silicides and determine their properties, such as (Schottky) barrier heights and contact resistances.[28,29] Knowledge of the growth pattern of coinage-metal-doped Si clusters will improve understanding of the formation mechanisms and associated properties of these silicides. For Si_nCu^+ ($n=6$–11), it is found that the Cu atom prefers to cap either a face or edge of the ground-state structure of the parent bare Si_n^+ or Si_n cluster.[26] In particular, Si_nCu^+ ($n=7$–9) retains the pentagonal bipyramid of the corresponding pure silicon clusters and a transition from a pentagonal bipyramidal motif to a trigonal prism-based structure occurs at $n=10$.[26] Experimentally, Jaeger et al. found that photodissociation of Si_nAg^+ ($n=7$ and 10) clusters proceeds primarily by the loss of metal atoms, thus indicating that silver–silicon bonds in the cluster are weaker than the silicon–silicon bonds.[30] Chuang et al. predicted by first-principles calculations that Si_nAg clusters ($n=1$–13) are all exohedral with the Ag atom capping the pure Si_n clusters.[31] Another computational study of geometries and electronic properties of Si_nAg ($n=1$–15) clusters has been carried out by Ziella et al.[32] In contrast to the work of Chuang et al., they found endohedral geometries for Si_nAg with $n>10$. Recently, Kong et al. investigated the structural evolution and electronic properties of Si_nAg^- ($n=3$–12) by using anion photoelectron spectroscopy in com-

[a] Y. Li, Prof. E. Janssens
Laboratory of Solid State Physics and Magnetism
KU Leuven, 3001 Leuven (Belgium)
E-mail: ewald.janssens@fys.kuleuven.be

[b] A. P. Woodham, Dr. A. Fielicke
Institut für Optik und Atomare Physik
Technische Universität Berlin, 10623 Berlin (Germany)
E-mail: fielicke@physik.tu-berlin.de

[c] Prof. J. T. Lyon
Department of Natural Sciences
Clayton State University, Morrow, Georgia 30260 (USA)

[d] Prof. J. T. Lyon, A. P. Woodham, Dr. A. Fielicke
Fritz-Haber-Institut der Max-Planck-Gesellschaft
14195 Berlin (Germany)

Supporting Information for this article is available on the WWW under http://dx.doi.org/10.1002/cphc.201300944.

bination with DFT calculations, and found that these clusters have exohedral structures with the Ag atom occupying a low coordinated site.[33] These contradicting findings demonstrate that, as yet, there is no conclusive understanding of the geometric structure of small Ag-doped Si_n clusters and the effect of Ag binding to $Si_n^{+/0/-}$ needs to be clarified.

In the present work, the geometric structures of Si_nAg^+ ($n=6$–15) clusters are assigned by a combination of experimental and theoretical investigations. The experimental spectra are obtained by IR-MPD spectroscopy on the corresponding cluster–xenon complexes and the theoretical results are calculated by DFT using the BP86 functional. These findings show that the Ag dopant atom in Si_nAg^+ ($n=6$–15) is located in an exohedral position. The growth mechanism of the clusters is discussed and compared with that of Si_nCu^+.

2. Results and Discussion

2.1. Mass Spectra

A typical mass spectrum of the $Si_nAg_m^+$ clusters and $Si_nAg_m^+ \cdot Xe_p$ complexes is presented in Figure 1. The Xe complexes are produced using a 0.3% ^{129}Xe in He mixture as the carrier gas. We observe Si_n^+, $Si_n^+ \cdot Xe$, Si_nAg^+ ($n \geq 6$), $Si_nAg^+ \cdot Xe$ ($n=1$–15), and $Si_nAg^+ \cdot Xe_2$ ($n=1$, 6–12) clusters under the given source conditions. The mass spectrometric signals are isotopically broadened, mainly from silicon, which has an isotopic distribution of 92.23 (^{28}Si), 4.67 (^{29}Si), and 3.10% (^{30}Si). To reduce the isotopic broadening, isotopically enriched ^{129}Xe is used instead of natural abundance Xe gas.

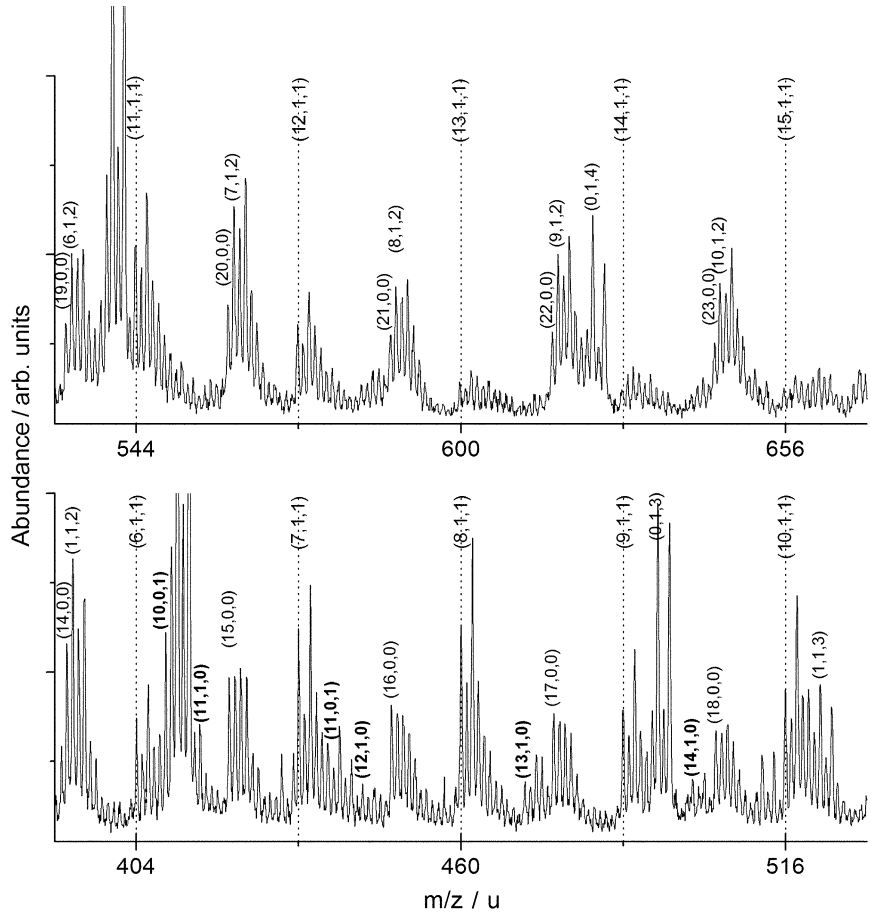

Figure 1. Typical mass spectrum of $Si_nAg_m^+ \cdot Xe_p$ clusters produced at a source temperature of 120 K using a 0.3% ^{129}Xe in He mixture as carrier gas. (n,m,p) are used to label the clusters. The labels are placed at the lightest isotope of each cluster.

2.2. Structural Assignment

Figures 2 and 3 show the experimental IR-MPD spectra of the rare-gas complexes $Si_nAg^+ \cdot Xe$ ($n=6$–15, there are no spectra obtained for $n=1$–5) and the theoretical IR spectra of the predicted lowest-energy isomers. For the larger sizes ($n=9$–15), low-lying isomers are also shown as they also provide reasonable agreement with the experimental spectra and therefore their presence cannot be excluded. A detailed comparison of the experimental spectra with computed spectra of various low-energy isomers is presented in the Supporting Information. All assigned isomers are closed shell, that is, have an electronic singlet state.

2.2.1. Si_6Ag^+

For Si_6Ag^+, the IR-MPD spectrum is characterized by one intense and broad band centered at approximately 440 cm^{-1} and an additional absorption around 525 cm^{-1}. These features are well reproduced by the calculated lowest-energy isomer with the Ag atom binding on top of the distorted octahedral structure of Si_6^+.[27] The calculated band around 430 cm^{-1} is actually composed of two bands with maxima at 428 and 434 cm^{-1} that are not resolved in the calculated IR spectrum because of an applied Gaussian broadening with a full width at half maximum of 8 cm^{-1}. These bands can explain the broad feature, which seems to have some substructure, in the experiment around 440 cm^{-1}. The weaker modes around 360 cm^{-1} do not show up in the experimental spectrum. Nevertheless, for bare Si_6Ag^+ we observe a significant signal increase around 370 cm^{-1}, which indicates the dissociation of a larger system (e.g. $Si_6Ag^+ \cdot Xe$) into Si_6Ag^+. The absence of this band in the experimental spectrum of $Si_6Ag^+ \cdot Xe$ could be due to the fragmentation of the heavier cluster $Si_6Ag^+ \cdot Xe_2$ (pres-

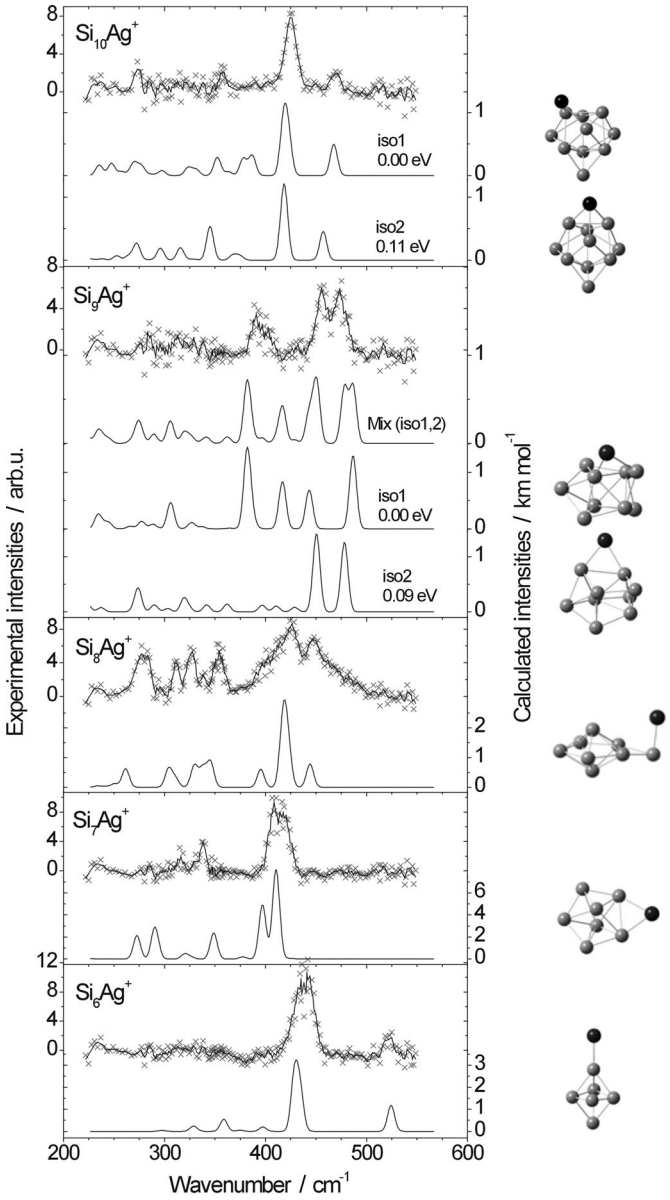

Figure 2. IR-MPD spectra (upper) of Si_nAg^+·Xe ($n = 6$–10) and the corresponding calculated IR spectra (lower) and geometric structures (right) of the obtained lowest-energy isomers. The crosses are the original data points, whereas the full lines correspond to three-point running averages.

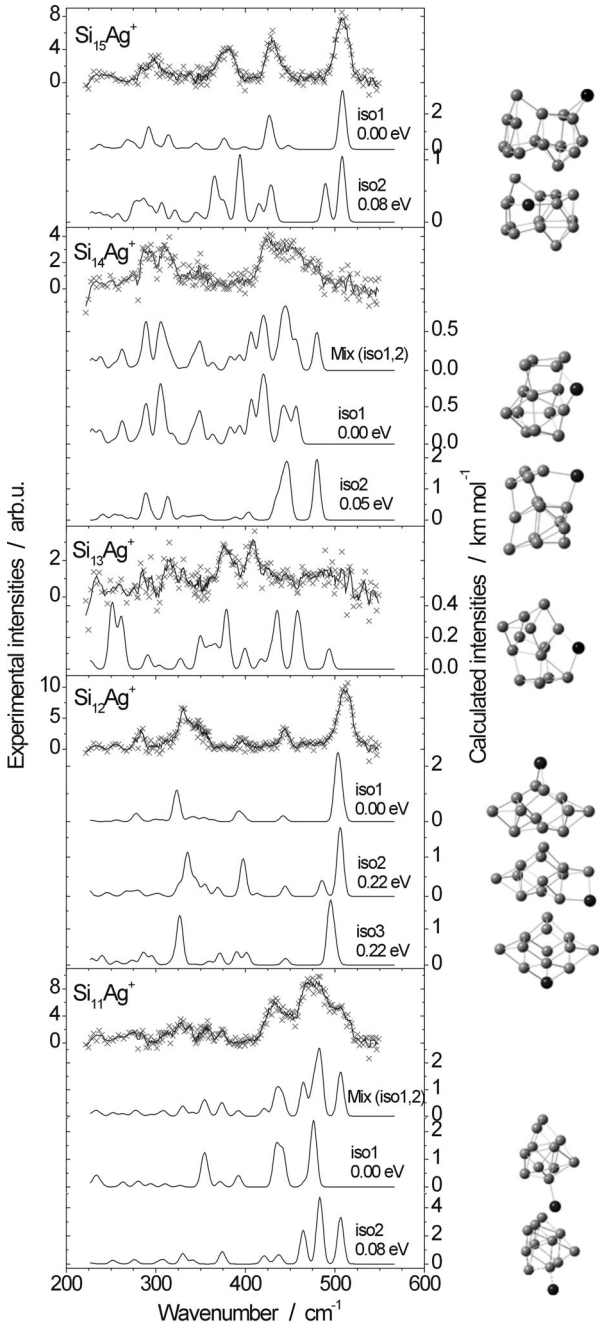

Figure 3. IR-MPD spectra (upper) of Si_nAg^+·Xe ($n = 11$–15) and the corresponding calculated IR spectra (lower) and geometric structures (right) of the best-fitting isomers.

ent as a small fraction in the molecular beam) at a similar wavelength, which obscures the depletion signal from Si_6Ag^+·Xe.

2.2.2. Si_7Ag^+

The experimental IR-MPD spectrum of Si_7Ag^+·Xe agrees quite well with the calculated IR spectrum of the lowest-energy isomer in the high-frequency region, which is dominated by two intense absorption bands centered at around 410 and 420 cm^{-1}, and several less intense bands towards lower frequency. The bands in the lowest-frequency region, between 270 and 290 cm^{-1}, are not as prominent in the experimental spectrum as predicted. It should be mentioned that for different functionals (BP86, B3P86, and B3LYP), the differences in frequencies of the normal vibrational modes are typically less than 10 cm^{-1} whereas the variations in the intensities of the different bands can be quite large. Further, although the attachment of noble-gas atoms to clusters typically has only little effect on the geometry of the cluster and thus the frequencies of the IR absorptions, it can affect the intensities.[27] The lowest-energy isomer of Si_7Ag^+ has the edge-capped pentagonal bipyramidal structure of Si_7^+[27] with the Ag atom at the equatorial position and was predicted previously.[31,32] This

structure is similar to that of the cationic Si_8^+[27] and to those of Si_7Cu^+[26] and Si_7Mn^+.[23]

2.2.3. Si_8Ag^+

The IR-MPD spectrum of Si_8Ag^+·Xe shows two broad bands between 410 and 450 cm^{-1}, and several lower-frequency bands between 260 and 360 cm^{-1}. Most bands are reasonably reproduced by the lowest-energy isomer, except for the lowest experimental band around 276 cm^{-1}, which is blueshifted relative to the computed one by approximately 16 cm^{-1}. The structure of this isomer is an edge-capped pentagonal bipyramid, in which Ag binds in an out-of-plane direction to the capping Si atom of the ground-state structure of Si_8^+.[27]

2.2.4. Si_9Ag^+

The IR-MPD spectrum of Si_9Ag^+·Xe shows two intense bands around 455 and 475 cm^{-1} and less intense features between 380 and 415 cm^{-1}. The lowest-energy isomer (**iso1**) reproduces several experimental features; however, the experimental highest-frequency mode (around 475 cm^{-1}) is redshifted by about 15 cm^{-1} relative to the calculation. This could be due to the influence of the Xe atom. The second lowest energy isomer (**iso2**), only 0.09 eV less stable than **iso1**, fits well with the high-frequency part of the experimental spectrum, although the band intensities around 380–415 cm^{-1} are lower than those in the experiment. Both **iso1** and **iso2** have bicapped pentagonal bipyramidal structures with the Ag atom capping at different positions, and both could be present in the cluster beam. A 1:1 mixture of the predicted spectra for **iso1** and **iso2** yields good agreement with the experimental spectrum. Multiple isomers could be present in the cluster beam because of the finite temperature of the clusters, which is assumed to be close to the source temperature of 120 K, and because of possible trapping of isomeric structures in local minima on the potential energy surface during the fast cooling process.

2.2.5. $Si_{10}Ag^+$

For $Si_{10}Ag^+$, the calculated lowest (**iso1**) and second lowest energy isomers (**iso2**, 0.11 eV higher in energy) have a similar tetracapped trigonal prism Si framework, with the Ag atom capping different positions. Their calculated IR spectra are also quite similar: as most of the vibrational modes in the experimental range are vibrations of the Si framework, the Ag–Si vibrational modes are at lower frequency (below 200 cm^{-1}). They both reproduce the experimental IR-MPD spectrum well, except that the small absorption feature around 360–375 cm^{-1} is not prominent in the experiment. However, for the bare $Si_{10}Ag^+$ clusters, we observe a weak signal increase around 370 cm^{-1}, which could come from the depletion of $Si_{10}Ag^+$·Xe. Again the depletion signal of $Si_{10}Ag^+$·Xe could be obscured (at least partially) by the fragmentation of $Si_{10}Ag^+$·Xe_2, thereby explaining the missing band in the experimental spectrum. Alternatively, this band is quite small and its intensity (or frequency) could be affected by the Xe attachment, as mentioned above.

2.2.6. $Si_{11}Ag^+$

The IR-MPD spectrum of $Si_{11}Ag^+$·Xe shows two broad features in the 415–520 cm^{-1} range and several smaller signals between 305 and 380 cm^{-1}. The spectrum of the most stable isomer of $Si_{11}Ag^+$ (**iso1**) fits the experiment best, although the calculated band around 355 cm^{-1} is less intense in the experiment and it is missing the highest-frequency band around 500 cm^{-1}. The second lowest energy isomer (**iso2**, 0.08 eV less stable) can also explain the experiment reasonably well. It has three intense peaks centered around 465, 483, and 505 cm^{-1}, which could correspond to the broad experimental features between 450 and 520 cm^{-1}. Similar to Si_9Ag^+, better agreement between experiment and theory is achieved if a 1:1 mixture of **iso1** and **iso2** is assumed. Both isomers have a pentacapped trigonal prism structure and can be transformed into each other by changing the position of a single Si atom.

2.2.7. $Si_{12}Ag^+$

For $Si_{12}Ag^+$, the IR-MPD spectrum of the corresponding Xe complexes depicts two strong absorptions around 330 and 510 cm^{-1} and three smaller bands around 280, 400, and 445 cm^{-1}. These features are well reproduced by the lowest-energy isomer of $Si_{12}Ag^+$, and even the relative intensities agree well. The silicon framework of this isomer contains a distorted tricapped trigonal prism building block, which was previously identified to be the ground-state structure of Si_{12}^+.[34] Isomers **iso2** and **iso3** show similar IR spectra to **iso1**. Their relative energies are comparatively high (+0.22 eV above **iso1**), but still close to the typical error of DFT methods (≈0.15 eV).[23–27,35,36] These two isomers cannot be ruled out, although their abundance in the molecular beam may be limited. Both of them have similar Si frameworks to **iso1**, but with the Ag atom capping at different positions.

2.2.8. $Si_{13}Ag^+$

For $Si_{13}Ag^+$, structural identification is difficult due to the poorer quality of the experimental spectrum and the emergence of many possible isomeric forms. More than 12 isomers of $Si_{13}Ag^+$ (see the Supporting Information) are located within a relative energy range of 0.4 eV. No compelling agreement, however, can be found between these isomers and the experiment. The Si framework of the obtained lowest-energy structure, **iso1**, has a two-layered structure (a rhombus and a pentagon). It has four intense bands around 250, 260, 435, and 458 cm^{-1}, and a broad feature between 320 and 400 cm^{-1}. The experimental spectrum, on the other hand, shows two intense bands around 375 and 408 cm^{-1}, and several small bands between 270 and 340 cm^{-1}. Other isomers always show high-frequency bands, which are not observed in the experiment. Therefore, no definitive assignment of the structure of $Si_{13}Ag^+$ can be made.

2.2.9. $Si_{14}Ag^+$

The IR-MPD spectrum of $Si_{14}Ag^+$·Xe has two broad features around 280–320 and 415–460 cm^{-1}, and a small one around 350 cm^{-1}. The calculated IR spectrum of the obtained lowest-energy isomer **iso1** of $Si_{14}Ag^+$ fits the experiment best. Its structure contains a multiply capped trigonal prism, albeit strongly distorted, with the Ag atom bridging one edge. **Iso2**, being only 0.05 eV higher in energy, also has a distorted trigonal prism-based structure. **Iso2** cannot be ruled out, as it has two small bands around 280 and 313 cm^{-1}, and three intense bands around 435, 446, and 480 cm^{-1}, consistent with the broad features of the experimental spectrum. Better agreement is achieved if a 3:1 mixture of **iso1** and **iso2** is assumed.

2.2.10. $Si_{15}Ag^+$

The IR-MPD spectrum of $Si_{15}Ag^+$·Xe shows four well-defined absorption bands around 300, 380, 430, and 510 cm^{-1}. The calculated spectrum of the lowest-energy isomer found fits best with the experiment, including the relative intensities of the absorption bands. However, the (additional) presence of **iso2** (0.08 eV higher in energy) cannot be fully excluded, although some of these predicted doublet bands are not resolved in the experiment. Both isomers have a similar Si framework to that of Si_{15}^+[27] with the Ag atom capping at different positions. For **iso1**, however, the Si structure is more strongly distorted.

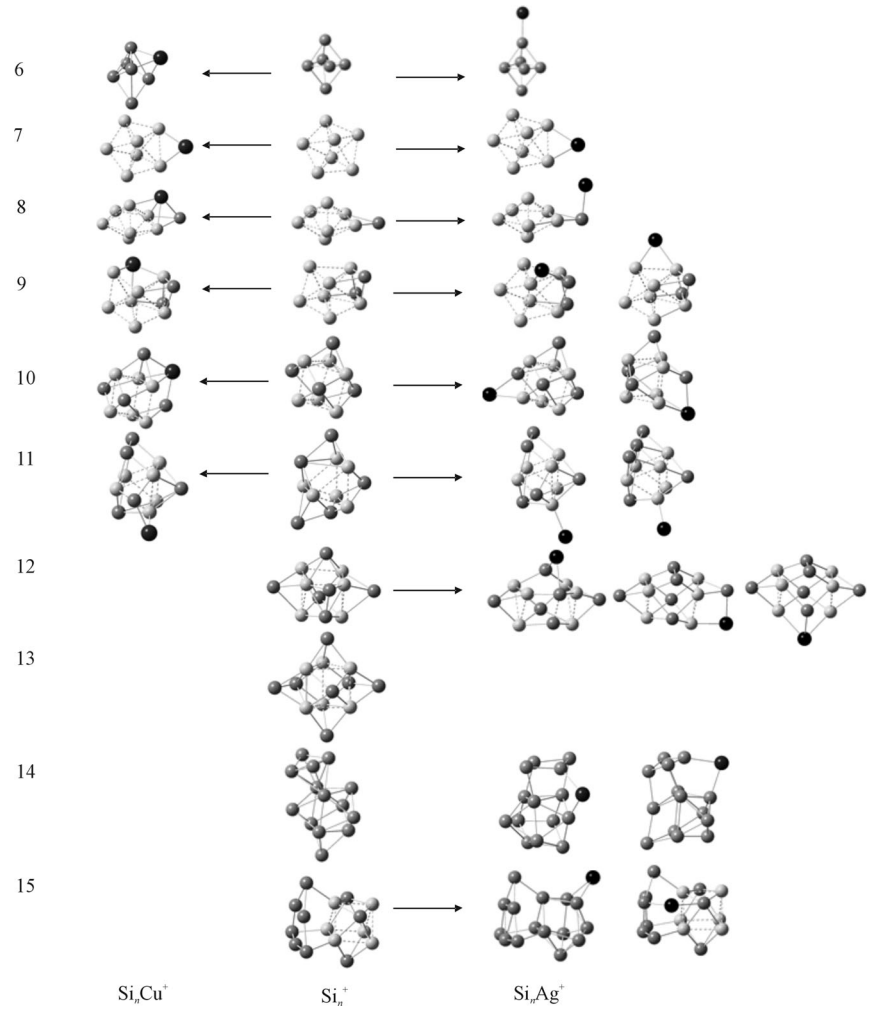

Figure 4. Growth mechanism of Si_nAg^+ clusters (right) in comparison with bare Si_n^+ (middle) and Si_nCu^+ clusters (left). Pentagonal bipyramid (n = 7–9) and trigonal prism building blocks (n = 10–15) are light shaded. The Ag and Cu dopant atoms are dark shaded. The structures of the Si_nCu^+ and Si_n^+ clusters are taken from refs. [26,27]. The structure of Si_{12}^+ is taken from ref. [34].

2.3. Growth Mechanism and Energetic Stabilities

The growth mechanism of Si_nAg^+ (n = 6–15) is illustrated in Figure 4 and compared with that of both bare Si_n^+[27] and copper-doped Si_nCu^+[26] clusters.

Based on the similar electronic structure of Cu and Ag atoms ($kd^{10}(k+1)s^1$), one may imagine that they would have a similar influence on the geometric structures of silicon clusters. Indeed, as we can see in Figure 4, they both like to adsorb to the Si_n^+ clusters in a low coordination site and the doped clusters follow similar growth patterns: retaining the pentagonal bipyramid for n = 7–9, whereas a transition to a trigonal prism motif seems to occur at n = 10. There are, however, also differences. For Si_6M^+ (M = metal), Cu likes to cap a face of Si_6^+, whereas Ag prefers to bind to an apex of Si_6^+,[27] an even lower coordinated position. Similar dopant-specific binding is found for Si_8M^+, Si_9M^+, and $Si_{10}M^+$: the Cu atom is added to an edge or bridges the apex silicon atoms, whereas Ag binds to an apex in Si_8Ag^+ and caps an edge in Si_9Ag^+ and $Si_{10}Ag^+$. It should be mentioned that the Si framework of Si_9Cu^+ is strongly distorted,[26] which indicates that the Cu atom has a stronger influence on the Si_n^+ clusters. For $Si_{11}M^+$, the Si frameworks are slightly different from the bare Si_{11}^+ clusters and Ag adsorbs to an apex of the trigonal prism building block, whereas Cu prefers to cap an edge. Interestingly, the structures of $Si_{11}Cu^+$ and $Si_{11}Ag^+$ are still quite similar. To summarize, the Ag dopant prefers to adsorb to the Si framework (apex or edge) in an even lower coordinated position than the Cu dopant atom (edge or face) as shown in Table 1.

For larger sizes, a similar comparison is not possible, since the structures of Si_nCu^+ (n = 12–15) are not known. Our previous investigations using argon physisorption as a structural

Table 1. Natural electronic configuration (NEC), the binding site (BS) of the dopant atoms, and the average binding energy per atom E_b [eV] of the Si_nAg^+ ($n=6$–15) and Si_nCu^+ ($n=6$–11) isomers shown in Figure 4.

Si_nCu^+[a]	NEC	BS	E_b	Si_nAg^+	NEC	BS	E_b
6	$3d^{9.84}4s^{0.494}p^{0.03}$	face	3.42	6	$4d^{9.92}5s^{0.49}p^{0.01}$	apex	3.33
7	$3d^{9.87}4s^{0.444}p^{0.02}$	edge	3.53	7	$4d^{9.90}5s^{0.47}p^{0.09}d^{0.01}$	edge	3.44
8	$3d^{9.82}4s^{0.544}p^{0.054}d^{0.01}$	face	3.49	8	$4d^{9.90}5s^{0.73}p^{0.04}$	apex	3.40
9	$3d^{9.82}4s^{0.574}p^{0.044}d^{0.01}$	face	3.56	9	$4d^{9.88}5s^{0.51}p^{0.06}d^{0.01}$	edge	3.49
10	$3d^{9.84}4s^{0.474}p^{0.034}d^{0.01}$	face	3.64	10	$4d^{9.90}5s^{0.44}p^{0.07}d^{0.01}$	edge	3.57
11	$3d^{9.82}4s^{0.544}p^{0.054}d^{0.01}$	edge	3.60	11	$4d^{9.92}5s^{0.60}p^{0.02}$	apex	3.56
				12	$4d^{9.88}5s^{0.56}p^{0.11}d^{0.02}$	edge	3.57
				13	$4d^{9.86}5s^{0.61}p^{0.14}d^{0.02}$	edge	3.58
				14	$4d^{9.88}5s^{0.55}p^{0.08}d^{0.02}$	edge	3.61
				15	$4d^{9.90}5s^{0.54}p^{0.08}d^{0.01}$	edge	3.62

[a] Ref. [26].

probe indicate that Si_nCu^+ clusters, from $n=12$ onwards, prefer to form endohedral metal-doped silicon cages.[19] Hagelberg et al. have shown that the neutral $Si_{12}Cu$ has a cagelike geometry, whereas the Cu atom in $Si_{10}Cu$ occupies a surface site.[11] Recently, Xu et al. conducted a combined anion photoelectron spectroscopy and DFT study on the structural evolution of copper-doped silicon clusters, Si_nCu^- ($n=4$–18), also indicating that the $n\geq12$ clusters are dominated by endohedral structures.[37] In contrast to this, the present work shows that the Si_nAg^+ ($n=12$–15) clusters have exohedral structures. This may be partially explained by the increase in atomic size of Ag relative to Cu. In particular, $Si_{12}Ag^+$ and $Si_{15}Ag^+$ can be obtained by capping the edge of bare Si_{12}^+[34] and Si_{15}^+,[27] respectively. The Si framework of $Si_{14}Ag^+$ differs from that of Si_{14}^+,[27] but still the Ag atom prefers to cap an edge. Most of the assigned structures of cationic Si_nAg^+ ($n=6$–12) in the work reported herein are not identical to those assigned for anionic Si_nAg^- ($n=6$–12) by Kong et al.,[33] but there is a general agreement in that the Ag atom prefers to be exohedral with a low coordinated position. The different charge states may explain the structural differences.

The natural electronic configuration, the binding site of the dopant atom, and the average binding energy per atom of Si_nAg^+ and Si_nCu^+ are listed in Table 1. It was shown earlier that the d orbitals of the transition metal play an important role in the binding site: the high coordination number for the V dopant atom in Si_nV^+ is related to its unfilled 3d orbitals, whereas Cu with filled 3d orbitals favors a lower coordination.[26] As shown in Table 1, the number of electrons in 4d orbitals of Ag is even slightly higher (9.9) than that in 3d orbitals of Cu (9.8). Because of its fully occupied 4d orbitals, Ag prefers to add to the bare Si clusters with an even lower coordinated position than Cu.

To further understand the stability of the transition-metal-doped silicon clusters, the average binding energies ($E_b(n)$) and fragmentation energies (D_1 and D_2) for different fragmentation channels were evaluated [Eqs. (1)–(3)]:

$$E_b(n) = [E(M^+)] + nE(Si) - E(Si_nM^+)]/(n+1) \quad (1)$$

$$D_1 = E(Si_n^+) + E(M) - E(Si_nM^+) \quad (2)$$

$$D_2 = E(Si_n) + E(M^+) - E(Si_nM^+) \quad (3)$$

in which $E(Si_n^+)$ and $E(Si_n)$ are the total energies of the ground-state structures. The lowest-energy structures of Si_n^+ ($n=6$–11, 13–15) are taken from ref. [27], and the structure of Si_{12}^+ is taken from ref. [34], but reoptimized at the level of theory used for the other sizes. The lowest-energy structures of Si_n ($n=6$–10, 15) are taken from refs. [35,36], and the structures of Si_n ($n=11$–14) are assumed to be similar to those of the corresponding cations, even though there is no experimental confirmation. $E(M^+)$ is obtained from $E(M)$ by adding the experimental ionization energy (7.58 eV for Ag and 7.73 eV for Cu). For Si_nAg^+ and Si_nCu^+, the structures as shown in Figure 4 are considered, and those of Si_nCu^+ are reoptimized and $E(Si_nCu^+)$ is recalculated at the present level of theory. Zero-point vibrational corrections are included in the total energies.

The size dependence of the fragmentation energy of Si_nCu^+ and Si_nAg^+ is depicted in Figure 5. It can be seen that the fragmentation energies of Si_nAg^+ are about 0.3–0.6 eV lower than those of Si_nCu^+. The difference between D_1 and D_2 equals the difference between the ionization energy of Si_n and that of the dopant atom. For small clusters $D_1 > D_2$, consistent with the ionization energy of small silicon clusters being higher than that of Ag and Cu. As the ionization energy of Si_n[38,39] clusters decreases with cluster size, D_1 becomes smaller than D_2 for larger sizes and the clusters prefer to dissociate by loss of

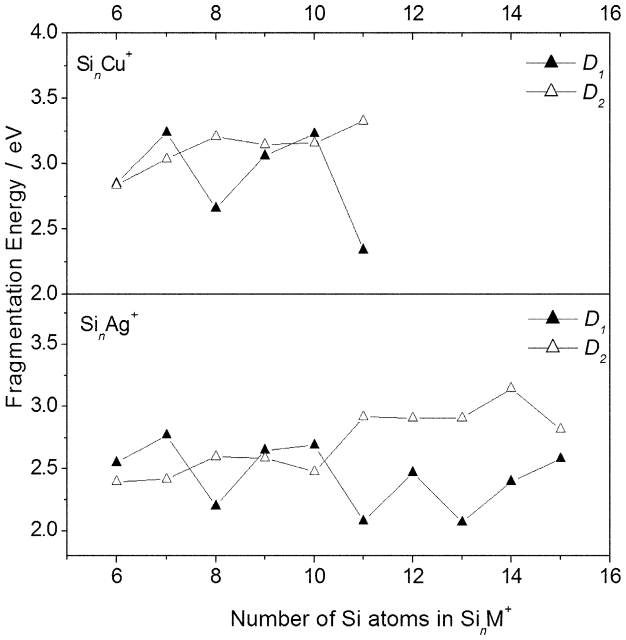

Figure 5. Size dependence of the fragmentation energy of Si_nAg^+ and Si_nCu^+.

a neutral dopant atom. Photodissociation data of Si_7Ag^+ and $Si_{10}Ag^+$ obtained by Jaeger et al.[30] indicate that the preferred dissociation channel of these sizes is through the loss of a neutral Ag atom, in disagreement with the results in Figure 5. The calculated energy difference between D_1 and D_2 is, however, small for these sizes. An overestimation of the calculated ionization energies for Si_n may be the origin of the discrepancy.

The size dependence of the average binding energy (E_b) of Si_nM^+ is shown in Figure 6. The binding energies of Si_nAg^+ are consistently lower than those of Si_nCu^+, thus indicating that the binding of silver to the silicon clusters is weaker than that of copper. This explanation is consistent with the preference

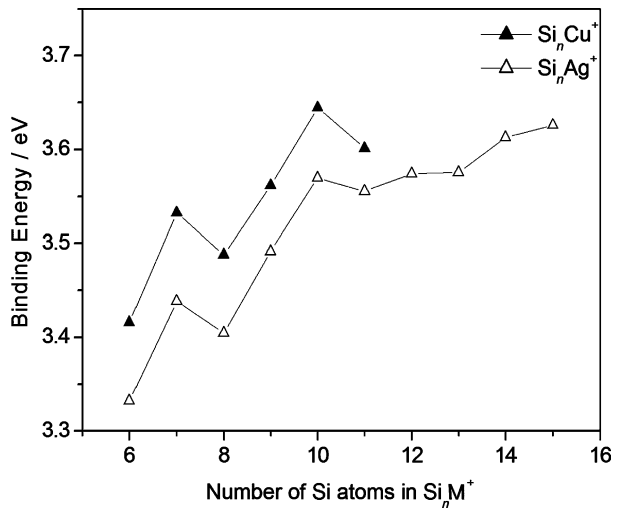

Figure 6. Size dependence of the average binding energy ($E_b(n)$) of Si_nAg^+ and Si_nCu^+.

for the Ag dopant to adsorb to the silicon frameworks in even lower coordinated positions and the structures of the Si_nAg^+ clusters are dominated by the Si_n^+ structures. Interestingly, in the size range $n=6$–11, the size dependence of both the fragmentation energy and binding energy shows a similar trend for Si_nAg^+ and Si_nCu^+. In particular, the binding energy curve reveals that Si_7M^+ and $Si_{10}M^+$ are more stable than the neighboring sizes.

It has been shown that the atomic radius of the dopant atom plays an important role in determining the critical size for cage formation of the transition-metal-doped Si clusters.[40] This critical size was found to decrease with the decreasing atomic radius of the 3d dopant atoms.[19] The atomic radius, however, cannot determine the critical size alone; the bonding properties and electronic structure (i.e. orbital hybridization between the dopant atoms and Si atoms) also have a significant influence on the growth pattern of the doped Si clusters.[41] The atomic radius difference between the Ag and Cu atoms indicates that more Si atoms are needed to encapsulate the Ag dopant; nevertheless, even for clusters as large as $Si_{15}Ag^+$, no cage formation is observed. The few isomers with endohedral structures that were located all have an energy much higher than the assigned ground state (see the Supporting Information). The similar growth patterns of smaller Si_nAg^+ and Si_nCu^+ indicate that the filled d orbitals may play an important role in the formation of exohedral structures. However, the caged structure of the $Si_{12}Cu$ cluster also shows an almost filled 3d orbital (9.87).[11] Compared with the bonding between Cu and Si atoms, the weaker Ag–Si bonds may account for the different growth patterns for larger sized Si_nAg^+ and Si_nCu^+ ($n=$ 12–15) with the Si atoms preferring to form bonds with each other instead of the Ag atom.[33]

3. Conclusions

In summary, we have assigned the geometric structures of Si_nAg^+ ($n=6$–15, with the exception of $n=13$) by a combination of experimental IR-MPD spectra measured on cluster–xenon complexes and theoretical IR spectra for various structural isomers. It is found that the Si_nAg^+ ($n=6$–15) clusters all have exohedral structures. The silicon framework in Si_7Ag^+, Si_8Ag^+, and Si_9Ag^+ is based on a pentagonal bipyramid, whereas a trigonal prism basis emerges for larger sizes ($n\geq 10$–12, 14, 15). Si_nAg^+ and Si_nCu^+ show a similar formation mechanism: both dopants like to adsorb to the Si cluster in a low coordinated position. There are also differences, however. In particular, compared to Cu-doped silicon clusters, the Ag atom has a smaller influence on the geometric structure of Si_n^+ clusters, and tends to adsorb to an apex or an edge of the ground-state structure of Si_n^+ at an even lower coordinated position than Cu. The binding energy of silver to the silicon clusters is weaker than that of copper. The different growth patterns for larger sized Si_nAg^+ and Si_nCu^+ ($n=12$–15) indicate that the atomic radius of the dopant atoms and bonding mechanism between metal dopant and Si play an important role in cage formation.

Experimental Section

Experimental Setup

The experiments were performed in a molecular beam setup[24] coupled to a beam line of the Free Electron Laser for Infrared eXperiments (FELIX) user facility at the FOM Institute for Plasma Physics, Nieuwegein, The Netherlands.[42] The clusters were produced in a dual-target laser vaporization cluster source at a repetition rate of 10 Hz, by ablating the target plates with the second harmonic output (532 nm, $\approx$20 mJ) of two pulsed Nd:YAG lasers.[43] Complexes with Xe were formed by condensation of the vaporized material in a short pulse of He gas containing a fraction ($\approx$0.3%) of isotopically enriched ^{129}Xe. The cluster formation channel was extended with a cooled copper channel maintained at about 120 K by a flow of liquid nitrogen. After expansion into vacuum the cluster distribution in the molecular beam was analyzed by using a reflectron time-of-flight mass spectrometer.

IR-MPD spectra were recorded by overlapping the molecular beam with the counter propagating intense infrared laser beam delivered by FELIX. The output of FELIX is tunable in the 40–2000 cm^{-1} range and consists of approximately 5–8 μs long macropulses with a typical energy of about 50 mJ. For the spectroscopy of the Ag-doped Si clusters in this experiment, FELIX was scanned over the range from 220 to 550 cm^{-1} with a step size of 3 cm^{-1}. The calibra-

tion uncertainty of the FELIX frequency amounted to 1–2 cm^{-1} in the studied range. Resonant absorption of the IR light by the cluster–rare gas complex heated the cluster and may have resulted in the dissociation of the xenon messenger atom, which was observed as a depletion of the ion intensity of the corresponding complex in the mass spectrum. IR depletion spectra of certain species were constructed by comparing the ion intensities of the cluster–xenon complex after exposure to FELIX with the non-irradiated ion intensities as a function of the FELIX frequency. Based on the depletion spectra, IR absorption spectra could be constructed as described previously.[24]

Theoretical Methods

Structural identification was obtained by comparison of the IR-MPD spectra with computed infrared spectra for different structural isomers. DFT calculations are currently the most important theoretical tool for the treatment of the transition-metal-doped clusters. The functional used for the DFT calculations in this work was BP-86 as implemented in the Gaussian program,[44] which has been shown to be successful for the structural assignment of Si_nV^+,[18] Si_nCu^+,[25,26] Si_n^+ ($n=6$–21),[27] and Si_n ($n=6$–10 and 15) clusters.[35,36] The SVP basis set was used for the Si atoms in combination with the SDD pseudopotential for Ag. Structures available in the literature for metal-doped silicon clusters were taken as initial configurations.[8,26,31,32] A global optimization basin-hopping approach on the BP-86/def-SVP level was applied to search for a large number of possible geometrical arrangements before tighter optimization; for details see ref. [45]. This turned out to be crucial especially in identifying the structures of the larger sizes due to the emergence of many possible isomeric forms. For each structure, spin multiplicities of $2s+1=1,3$ were considered. Consistent with earlier work on pure and doped silicon clusters, the calculated harmonic vibrational frequencies were scaled with a constant multiplication factor of 1.03,[25–27,35,36] and peaks were given a full width at half maximum of 8 cm^{-1}.

Acknowledgements

The authors thank Peter Lievens for stimulating discussions. They gratefully acknowledge the support of the Stichting voor Fundamenteel Onderzoek der Materie (FOM) in providing beam time on FELIX and highly appreciate the skillful assistance of the FELIX staff. This work is supported by the European Community's FP7/2007–2013 (Grant No. 226716), the Research Foundation–Flanders (FWO), the KU Leuven Research Council (GOA program), and the Deutsche Forschungsgemeinschaft within FOR 1282 (FI 893/4). J.T.L. is grateful to the Alexander von Humboldt Foundation and the donors of the American Chemical Society Petroleum Research Fund for support of this research. This work used the Extreme Science and Engineering Discovery Environment (XSEDE), which is supported by National Science Foundation grant number OCI-1053575.

Keywords: cluster compounds · density functional calculations · IR spectroscopy · silicon · silver

[1] K. Raghavachari, V. Logovinsky, *Phys. Rev. Lett.* **1985**, *55*, 2853–2856.
[2] W. L. Brown, R. R. Freeman, K. Raghavachari, M. Schluter, *Science* **1987**, *235*, 860–865.
[3] E. C. Honea, A. Ogura, C. A. Murray, K. Raghavachari, W. O. Sprenger, M. F. Jarrold, W. L. Brown, *Nature* **1993**, *366*, 42–44.
[4] G. S. Icking-Konert, H. Handschuh, P. S. Bechthold, G. Gantefor, B. Kessler, W. Eberhardt, *Surf. Rev. Lett.* **1996**, *3*, 483–487.
[5] K. M. Ho, A. A. Shvartsburg, B. C. Pan, Z. Y. Lu, C. Z. Wang, J. G. Wacker, J. L. Fye, M. F. Jarrold, *Nature* **1998**, *392*, 582–585.
[6] A. A. Shvartsburg, R. R. Hudgins, P. Dugourd, M. F. Jarrold, *Chem. Soc. Rev.* **2001**, *30*, 26–35.
[7] J. M. Antonietti, F. Conus, A. Chatelain, S. Fedrigo, *Phys. Rev. B* **2003**, *68*, 035420.
[8] J. Wang, Y. Liu, Y. C. Li, *Phys. Lett. A* **2010**, *374*, 2736–2742.
[9] S. Goedecker, W. Hellmann, T. Lenosky, *Phys. Rev. Lett.* **2005**, *95*, 055501.
[10] X. Zhu, X. C. Zeng, *J. Chem. Phys.* **2003**, *118*, 3558–3570.
[11] C. Xiao, F. Hagelberg, Jr., W. A. Lester, *Phys. Rev. B* **2002**, *66*, 075425.
[12] S. Nigam, C. Majumder, S. K. Kulshreshtha, *J. Chem. Phys.* **2004**, *121*, 7756–7763.
[13] S. Wei, R. N. Barnett, U. Landman, *Phys. Rev. B* **1997**, *55*, 7935–7944.
[14] A. D. Zdetsis, *J. Chem. Phys.* **2007**, *127*, 244308.
[15] R. Kishi, Y. Negishi, H. Kawamata, S. Iwata, A. Nakajima, K. Kaya, *J. Chem. Phys.* **1998**, *108*, 8039–8048.
[16] U. Röthlisberger, W. Andreoni, M. Parrinello, *Phys. Rev. Lett.* **1994**, *72*, 665–668.
[17] K. Jackson, B. Nellermoe, *Chem. Phys. Lett.* **1996**, *254*, 249–256.
[18] P. Claes, E. Janssens, V. T. Ngan, P. Gruene, J. T. Lyon, D. J. Harding, A. Fielicke, M. T. Nguyen, P. Lievens, *Phys. Rev. Lett.* **2011**, *107*, 173401.
[19] E. Janssens, P. Gruene, G. Meijer, L. Woste, P. Lievens, A. Fielicke, *Phys. Rev. Lett.* **2007**, *99*, 063401.
[20] K. Koyasu, M. Akutsu, M. Mitsui, A. Nakajima, *J. Am. Chem. Soc.* **2005**, *127*, 4998–4999.
[21] J. T. Lau, K. Hirsch, Ph. Klar, A. Langenberg, F. Lofink, R. Richter, J. Rittmann, M. Vogel, V. Zamudio-Bayer, T. Möller, *Phys. Rev. A* **2009**, *79*, 053201.
[22] V. Kumar, *Comput. Mater. Sci.* **2006**, *36*, 1–11.
[23] V. T. Ngan, E. Janssens, P. Claes, J. T. Lyon, A. Fielicke, M. T. Nguyen, P. Lievens, *Chem. Eur. J.* **2012**, *18*, 15788–15793.
[24] A. Fielicke, G. von Helden, G. Meijer, *Eur. Phys. J. D* **2005**, *34*, 83–88.
[25] P. Gruene, A. Fielicke, G. Meijer, E. Janssens, V. T. Ngan, M. T. Nguyen, P. Lievens, *ChemPhysChem* **2008**, *9*, 703–706.
[26] V. T. Ngan, P. Gruene, P. Claes, E. Janssens, A. Fielicke, M. T. Nguyen, P. Lievens, *J. Am. Chem. Soc.* **2010**, *132*, 15589–15602.
[27] J. T. Lyon, P. Gruene, A. Fielicke, G. Meijer, E. Janssens, P. Claes, P. Lievens, *J. Am. Chem. Soc.* **2009**, *131*, 1115–1121.
[28] M. Setton, J. Van der Spiegel, B. Rothman, *Appl. Phys. Lett.* **1990**, *57*, 357–359.
[29] S. Hymes, S. P. Muraka, C. Shepard, W. A. Langford, *J. Appl. Phys.* **1992**, *71*, 4623–4625.
[30] J. B. Jaeger, T. D. Jaeger, M. A. Duncan, *J. Phys. Chem. A* **2006**, *110*, 9310–9314.
[31] F. C. Chuang, Y. Y. Hsieh, C. H. Hus, M. A. Albao, *J. Chem. Phys.* **2007**, *127*, 144313.
[32] D. H. Ziella, M. C. Caputo, P. F. Provasi, *Int. J. Quantum Chem.* **2011**, *111*, 1680–1693.
[33] X. Y. Kong, X. J. Deng, H. G. Xu, Z. Yang, X. L. Xu, W. J. Zheng, *J. Chem. Phys.* **2013**, *138*, 244312.
[34] M. Vogel, C. Kasigkeit, K. Hirsch, A. Langenberg, J. Rittmann, V. Zamudio-Bayer, A. Kulesza, R. Mitrić, T. Möller, B. von Issendorff, J. T. Lau, *Phys. Rev. B* **2012**, *85*, 195454.
[35] M. Haertelt, J. T. Lyon, P. Claes, J. de Haeck, P. Lievens, *J. Chem. Phys.* **2012**, *136*, 064301.
[36] A. Fielicke, J. T. Lyon, M. Haertelt, G. Meijer, P. Claes, J. de Haeck, P. Lievens, *J. Chem. Phys.* **2009**, *131*, 171105.
[37] H. G. Xu, M. M. Wu, Z. G. Zhang, J. Y. Yuan, Q. Sun, *J. Chem. Phys.* **2012**, *136*, 104308.
[38] K. Fuke, K. Tsukamoto, F. Misaizu, M. Sanekata, *J. Chem. Phys.* **1993**, *99*, 7807–7812.
[39] O. Kostko, S. R. Leone, M. A. Duncan, M. Ahmed, *J. Chem. Phys.* **2010**, *114*, 3176–3181.
[40] L. Ma, J. J. Zhao, J. G. Wang, B. L. Wang, Q. L. Lu, G. H. Wang, *Phys. Rev. B* **2006**, *73*, 125439.
[41] L. J. Guo, G. F. Zhao, Y. Z. Gu, X. Liu, Z. Zeng, *Phys. Rev. B* **2008**, *77*, 195417.

[42] D. Oepts, A. F. G. van der Meer, P. W. van Amersfoort, *Infrared Phys. Technol.* **1995**, *36*, 297 – 308.
[43] W. Bouwen, P. Thoen, F. Vanhoutte, S. Bouckaert, F. Despa, H. Weidele, R. E. Silverans, P. Lievens, *Rev. Sci. Instrum.* **2000**, *71*, 54 – 58.
[44] Gaussian 09 (Revision D.01), M. J. Frisch, G. W. Trucks, H. B. Schlegel, G. E. Scuseria, M. A. Robb, J. R. Cheeseman, G. Scalmani, V. Barone, B. Mennucci, G. A. Petersson, H. Nakatsuji, M. Caricato, X. Li, H. P. Hratchian, A. F. Izmaylov, J. Bloino, G. Zheng, J. L. Sonnenberg, M. Hada, M. Ehara, K. Toyota, R. Fukuda, J. Hasegawa, M. Ishida, T. Nakajima, Y. Honda, O. Kitao, H. Nakai, T. Vreven, J. A. Montgomery, Jr., J. E. Peralta, F. Ogliaro, M. Bearpark, J. J. Heyd, E. Brothers, K. N. Kudin, V. N. Staroverov, T. Keith, R. Kobayashi, J. Normand, K. Raghavachari, A. Rendell, J. C. Burant, S. S. Iyengar, J. Tomasi, M. Cossi, N. Rega, J. M. Millam, M. Klene, J. E. Knox, J. B. Cross, V. Bakken, C. Adamo, J. Jaramillo, R. Gomperts, R. E. Stratmann, O. Yazyev, A. J. Austin, R. Cammi, C. Pomelli, J. W. Ochterski, R. L. Martin, K. Morokuma, V. G. Zakrzewski, G. A. Voth, P. Salvador, J. J. Dannenberg, S. Dapprich, A. D. Daniels, O. Farkas, J. B. Foresman, J. V. Ortiz, J. Cioslowski, D. J. Fox, Gaussian, Inc., Wallingford, CT, **2013**.
[45] D. J. Harding, C. Kerpal, G. Meijer, A. Fielicke, *J. Phys. Chem. Lett.* **2013**, *4*, 892 – 896.

Received: October 14, 2013
Published online on ■■ ■■, 2013

ARTICLES

Y. Li, J. T. Lyon, A. P. Woodham, A. Fielicke, E. Janssens**

■■ – ■■

The Geometric Structure of Silver-Doped Silicon Clusters

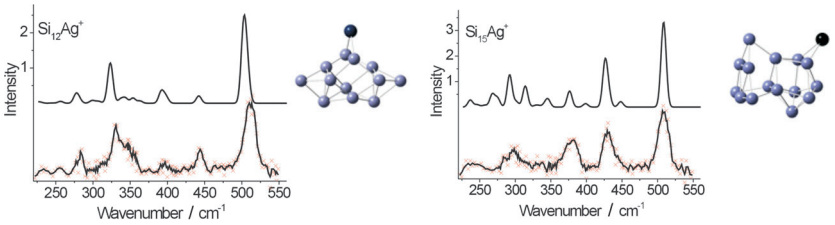

Coining it in: The geometric structures of Si_nAg^+ clusters are studied by infrared multiple photon dissociation in combination with density functional theory computations (see picture). The Si_nAg^+ ($n = 6$–15) clusters all have exohedral structures and the Ag dopant prefers to adsorb to the Si cluster at a low coordinated position.